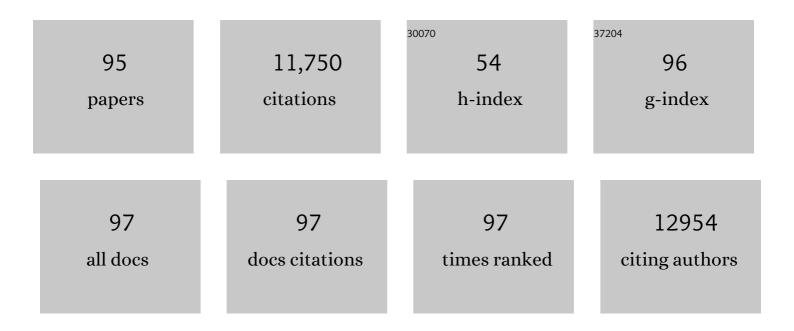
List of Publications by Year in descending order

Source: https://exaly.com/author-pdf/323959/publications.pdf Version: 2024-02-01



#	Article	IF	CITATIONS
1	Selective photocatalytic oxidation of gaseous ammonia at ppb level over Pt and F modified TiO2. Applied Catalysis B: Environmental, 2022, 300, 120688.	20.2	30
2	Engineering metal-organic frameworks for efficient photocatalytic conversion of CO2 into solar fuels. Coordination Chemistry Reviews, 2022, 450, 214245.	18.8	64
3	Extracellular proteins of Desulfovibrio vulgaris as adsorbents and redox shuttles promote biomineralization of antimony. Journal of Hazardous Materials, 2022, 426, 127795.	12.4	13
4	Recovering solar fuels from photocatalytic CO2 reduction over W6+-incorporated crystalline g-C3N4 nanorods by synergetic modulation of active centers. Applied Catalysis B: Environmental, 2022, 304, 120978.	20.2	88
5	iTRAQ-derived quantitative proteomics uncovers the neuroprotective property of bexarotene in a mice model of cerebral ischemia–reperfusion injury. Saudi Pharmaceutical Journal, 2022, 30, 585-594.	2.7	3
6	Two-Dimensional High-Entropy Metal Phosphorus Trichalcogenides for Enhanced Hydrogen Evolution Reaction. ACS Nano, 2022, 16, 3593-3603.	14.6	77
7	β-Caryophyllene suppresses ferroptosis induced by cerebral ischemia reperfusion via activation of the NRF2/HO-1 signaling pathway in MCAO/R rats. Phytomedicine, 2022, 102, 154112.	5.3	41
8	2D Transition Metal Dichalcogenides: Design, Modulation, and Challenges in Electrocatalysis. Advanced Materials, 2021, 33, e1907818.	21.0	284
9	Electrocatalysts: 2D Transition Metal Dichalcogenides: Design, Modulation, and Challenges in Electrocatalysis (Adv. Mater. 6/2021). Advanced Materials, 2021, 33, 2170045.	21.0	9
10	Differentially expressed genes induced by β-caryophyllene in a rat model of cerebral ischemia-reperfusion injury. Life Sciences, 2021, 273, 119293.	4.3	9
11	Synergetic Molecular Oxygen Activation and Catalytic Oxidation of Formaldehyde over Defective MIL-88B(Fe) Nanorods at Room Temperature. Environmental Science & Technology, 2021, 55, 8341-8350.	10.0	98
12	Synergetic surface modulation of ZnO/Pt@ZIF-8 hybrid nanorods for enhanced photocatalytic CO2 valorization. Applied Catalysis B: Environmental, 2021, 287, 119934.	20.2	91
13	Controlled Synthesis of Hollow Bimetallic Prussian Blue Analog for Conversion into Efficient Oxygen Evolution Electrocatalyst. ACS Sustainable Chemistry and Engineering, 2020, 8, 1319-1328.	6.7	39
14	Formation of assimilable organic carbon (AOC) during drinking water disinfection: A microbiological prospect of disinfection byproducts. Environment International, 2020, 135, 105389.	10.0	33
15	Ternary g <sub>3</sub> N <sub>4</sub> /ZnNCN@ZIFâ€8 Hybrid Photocatalysts with Robust Interfacial Interactions and Enhanced CO <sub>2</sub> Reduction Performance. Solar Rrl, 2020, 4, 1900440.	5.8	49
16	Bifunctional S-scheme g-C3N4/Bi/BiVO4 hybrid photocatalysts toward artificial carbon cycling. Chinese Journal of Catalysis, 2020, 41, 140-153.	14.0	204
17	Hydrogen producing water treatment through mesoporous TiO2 nanofibers with oriented nanocrystals. Chinese Journal of Catalysis, 2020, 41, 50-61.	14.0	46
18	Different effects of fluoride and phosphate anions on TiO <sub>2</sub> photocatalysis (rutile). Catalysis Science and Technology, 2020, 10, 6552-6561.	4.1	15

#	Article	IF	CITATIONS
19	Hydrogen production from natural organic matter via cascading oxic-anoxic photocatalytic processes: An energy recovering water purification technology. Water Research, 2020, 175, 115684.	11.3	23
20	Enhancing and Complementary Mechanisms of Synergistic Action of Acori Tatarinowii Rhizoma and Codonopsis Radix for Alzheimer's Disease Based on Systems Pharmacology. Evidence-based Complementary and Alternative Medicine, 2020, 2020, 1-26.	1.2	4
21	Effects of fluorine on photocatalysis. Chinese Journal of Catalysis, 2020, 41, 1451-1467.	14.0	96
22	Enhancing the room-temperature catalytic degradation of formaldehyde through constructing surface lewis pairs on carbon-based catalyst. Applied Catalysis B: Environmental, 2020, 272, 118992.	20.2	38
23	Efficient transformative HCHO capture by defective NH <sub>2</sub> -UiO-66(Zr) at room temperature. Environmental Science: Nano, 2019, 6, 2931-2936.	4.3	38
24	Positive effect of Fe <sup>3+</sup> ions on Bi <sub>2</sub> WO <sub>6</sub> , Bi <sub>2</sub> MoO <sub>6</sub> and BiVO <sub>4</sub> photocatalysis for phenol oxidation under visible light. Catalysis Science and Technology, 2019, 9, 4413-4421.	4.1	19
25	Role of Ni2+ ions in TiO2 and Pt/TiO2 photocatalysis for phenol degradation in aqueous suspensions. Applied Catalysis B: Environmental, 2019, 258, 117903.	20.2	34
26	Bexarotene Attenuates Focal Cerebral Ischemia–Reperfusion Injury via the Suppression of JNK/Caspase-3 Signaling Pathway. Neurochemical Research, 2019, 44, 2809-2820.	3.3	16
27	Boosting Hydrogen Transfer during Volmer Reaction at Oxides/Metal Nanocomposites for Efficient Alkaline Hydrogen Evolution. ACS Energy Letters, 2019, 4, 3002-3010.	17.4	142
28	Co-doped MgAl-LDHs nanosheets supported Au nanoparticles for complete catalytic oxidation of HCHO at room temperature. Applied Surface Science, 2019, 487, 260-271.	6.1	59
29	Beyond 1Tâ€phase? Synergistic Electronic Structure and Defects Engineering in 2Hâ€MoS <sub>2x</sub> Se <sub>2(1â€x)</sub> Nanosheets for Enhanced Hydrogen Evolution Reaction and Sodium Storage. ChemCatChem, 2019, 11, 3200-3211.	3.7	21
30	Single-crystalline melem (C <sub>6</sub> N <sub>10</sub> H <sub>6</sub> ) nanorods: a novel stable molecular crystal photocatalyst with modulated charge potentials and dynamics. Journal of Materials Chemistry A, 2019, 7, 13234-13241.	10.3	22
31	Synergetic degradation of VOCs by vacuum ultraviolet photolysis and catalytic ozonation over Mn-xCe/ZSM-5. Journal of Hazardous Materials, 2019, 364, 770-779.	12.4	74
32	Three-dimensional α-Fe2O3/amino-functionalization carbon nanotube sponge for adsorption and oxidative removal of tetrabromobisphenol A. Separation and Purification Technology, 2019, 211, 359-367.	7.9	36
33	Larger Adsorption Effect of Fluoride than Phosphate on Phenol Degradation over the Irradiated Anatase TiO <sub>2</sub> and Pt/TiO <sub>2</sub> . Acta Chimica Sinica, 2019, 77, 351.	1.4	1
34	Cationic nickel metal-organic frameworks for adsorption of negatively charged dye molecules. Data in Brief, 2018, 18, 1952-1961.	1.0	14
35	Selective and adsorptive removal of anionic dyes and CO2 with azolium-based metal-organic frameworks. Journal of Colloid and Interface Science, 2018, 519, 214-223.	9.4	41
36	TiO2 nanodots anchored on nitrogen-doped carbon nanotubes encapsulated cobalt nanoparticles as photocatalysts with photo-enhanced catalytic activity towards the pollutant removal. Journal of Colloid and Interface Science, 2018, 526, 158-166.	9.4	32

#	Article	IF	CITATIONS
37	MOFâ€Based Transparent Passivation Layer Modified ZnO Nanorod Arrays for Enhanced Photoâ€Electrochemical Water Splitting. Advanced Energy Materials, 2018, 8, 1800101.	19.5	143
38	Promotional role of Mn doping on catalytic oxidation of VOCs over mesoporous TiO2 under vacuum ultraviolet (VUV) irradiation. Applied Catalysis B: Environmental, 2018, 220, 78-87.	20.2	95
39	Enhanced photocatalytic CO <sub>2</sub> valorization over TiO <sub>2</sub> hollow microspheres by synergetic surface tailoring and Au decoration. Journal of Materials Chemistry A, 2018, 6, 24245-24255.	10.3	113
40	Synergetic tuning charge dynamics and potentials of Ag3PO4 photocatalysts with boosting activity and stability by facile in-situ fluorination. Applied Surface Science, 2018, 455, 1137-1149.	6.1	42
41	Sustained production of H2O2 in alkaline water solution using borate and phosphate-modified Au/TiC2 photocatalysts. Photochemical and Photobiological Sciences, 2018, 17, 1018-1022.	2.9	27
42	Degradation of TBBPA and BPA from aqueous solution using organo-montmorillonite supported nanoscale zero-valent iron. Chemical Engineering Journal, 2017, 309, 717-724.	12.7	72
43	Performance and Mechanism of Piezo-Catalytic Degradation of 4-Chlorophenol: Finding of Effective Piezo-Dechlorination. Environmental Science & Technology, 2017, 51, 6560-6569.	10.0	245
44	Activation of peroxymonosulfate by nitrogen-functionalized sludge carbon for efficient degradation of organic pollutants in water. Bioresource Technology, 2017, 241, 244-251.	9.6	124
45	Efficient degradation of tetrabromobisphenol A by synergistic integration of Fe/Ni bimetallic catalysis and microbial acclimation. Water Research, 2017, 122, 471-480.	11.3	52
46	Enhanced photocatalytic conversion of greenhouse gas CO2 into solar fuels over g-C3N4 nanotubes with decorated transparent ZIF-8 nanoclusters. Applied Catalysis B: Environmental, 2017, 211, 1-10.	20.2	298
47	Effect of F-Doping on the Photocatalytic Activity and Microstructures of Nanocrystalline TiO2 Powders. Nanostructure Science and Technology, 2016, , 187-200.	0.1	3
48	Fabrication and enhanced CO2 reduction performance of N-self-doped TiO2 microsheet photocatalyst by bi-cocatalyst modification. Journal of CO2 Utilization, 2016, 16, 442-449.	6.8	99
49	ZIF-8 derived bimodal carbon modified ZnO photocatalysts with enhanced photocatalytic CO <sub>2</sub> reduction performance. RSC Advances, 2016, 6, 59998-60006.	3.6	64
50	Efficient removal of gaseous formaldehyde in air using hierarchical titanate nanospheres with in situ amine functionalization. Physical Chemistry Chemical Physics, 2016, 18, 18161-18168.	2.8	30
51	Nitrogen-doped TiO2 microsheets with enhanced visible light photocatalytic activity for CO2 reduction. Chinese Journal of Catalysis, 2015, 36, 2127-2134.	14.0	197
52	Ternary reduced-graphene-oxide/Bi2MoO6/Au nanocomposites withÂenhanced photocatalytic activity under visible light. Journal of Alloys and Compounds, 2015, 649, 28-34.	5.5	57
53	Amine-Functionalized Titanate Nanosheet-Assembled Yolk@Shell Microspheres for Efficient Cocatalyst-Free Visible-Light Photocatalytic CO <sub>2</sub> Reduction. ACS Applied Materials & Interfaces, 2015, 7, 8166-8175.	8.0	128
54	Facile synthesis of few-layer-thick carbon nitride nanosheets by liquid ammonia-assisted lithiation method and their photocatalytic redox properties. RSC Advances, 2014, 4, 32690-32697.	3.6	63

#	Article	IF	CITATIONS
55	Porous Fluorinated SnO <sub>2</sub> Hollow Nanospheres: Transformative Self-assembly and Photocatalytic Inactivation of Bacteria. ACS Applied Materials & Interfaces, 2014, 6, 2407-2414.	8.0	72
56	Enhanced photocatalytic H <sub>2</sub> -production activity of TiO <sub>2</sub> using Ni(NO <sub>3</sub> ) <sub>2</sub> as an additive. Physical Chemistry Chemical Physics, 2013, 15, 12033-12039.	2.8	79
57	Ionicâ€Liquidâ€Assisted Synthesis of Uniform Fluorinated B/Câ€Codoped TiO <sub>2</sub> Nanocrystals and Their Enhanced Visibleâ€Light Photocatalytic Activity. Chemistry - A European Journal, 2013, 19, 2433-2441.	3.3	147
58	Tandem photocatalytic oxidation of Rhodamine B over surface fluorinated bismuth vanadate crystals. Journal of Materials Chemistry, 2012, 22, 17759.	6.7	114
59	Enhanced photovoltaic performance of dye-sensitized solar cells based on TiO2 nanosheets/graphene composite films. Journal of Materials Chemistry, 2012, 22, 17027.	6.7	200
60	Unique photocatalytic oxidation reactivity and selectivity of TiO2–graphene nanocomposites. Nanoscale, 2012, 4, 3193.	5.6	176
61	Fluorinated semiconductor photocatalysts: Tunable synthesis and unique properties. Advances in Colloid and Interface Science, 2012, 173, 35-53.	14.7	159
62	Enhanced photocatalytic activity of mesoporous TiO <sub>2</sub> aggregates by embedding carbon nanotubes as electron-transfer channel. Physical Chemistry Chemical Physics, 2011, 13, 3491-3501.	2.8	476
63	Improved visible-light photocatalytic activity of porous carbon self-doped ZnO nanosheet-assembled flowers. CrystEngComm, 2011, 13, 2533.	2.6	328
64	A simple cation exchange approach to Bi-doped ZnS hollow spheres with enhanced UV and visible-light photocatalytic H2-production activity. Journal of Materials Chemistry, 2011, 21, 14655.	6.7	203
65	Anatase TiO <sub>2</sub> with Dominant High-Energy {001} Facets: Synthesis, Properties, and Applications. Chemistry of Materials, 2011, 23, 4085-4093.	6.7	669
66	Ag <sub>2</sub> O as a New Visible‣ight Photocatalyst: Selfâ€Stability and High Photocatalytic Activity. Chemistry - A European Journal, 2011, 17, 7777-7780.	3.3	423
67	Superparamagnetic γ-Fe2O3@SiO2@TiO2 composite microspheres with superior photocatalytic properties. Applied Catalysis B: Environmental, 2011, 104, 12-20.	20.2	209
68	Low-temperature hydrothermal synthesis of highly photoactive mesoporous spherical TiO2 nanocrystalline. Journal of Physics and Chemistry of Solids, 2010, 71, 507-510.	4.0	20
69	Ion-Exchange Synthesis and Enhanced Visible-Light Photoactivity of CuS/ZnS Nanocomposite Hollow Spheres. Journal of Physical Chemistry C, 2010, 114, 13642-13649.	3.1	274
70	In-Flight Formation of Nano-Crystalline Titanium Dioxide Powder in a Plasma Jet and Its Characterization. Plasma Science and Technology, 2010, 12, 426-432.	1.5	5
71	Tunable Photocatalytic Selectivity of Hollow TiO <sub>2</sub> Microspheres Composed of Anatase Polyhedra with Exposed {001} Facets. Journal of the American Chemical Society, 2010, 132, 11914-11916.	13.7	979
72	Effects of annealing on the microstructures and photoactivity of fluorinated N-doped TiO2. Physical Chemistry Chemical Physics, 2010, 12, 12308.	2.8	96

#	Article	IF	CITATIONS
73	Characterization and visible light photocatalytic properties of nanocrystalline TiO2 synthesized by reactive plasma processing. Solar Energy Materials and Solar Cells, 2009, 93, 1540-1549.	6.2	27
74	Hydrothermal preparation and photocatalytic activity of mesoporous Au–TiO2 nanocomposite microspheres. Journal of Colloid and Interface Science, 2009, 334, 58-64.	9.4	200
75	Spray-hydrolytic synthesis of highly photoactive mesoporous anatase nanospheres for the photocatalytic degradation of toluene in air. Applied Catalysis B: Environmental, 2009, 89, 160-166.	20.2	58
76	Synergetic Codoping in Fluorinated Ti <sub>1â^'<i>x</i></sub> Zr <sub><i>x</i></sub> O <sub>2</sub> Hollow Microspheres. Journal of Physical Chemistry C, 2009, 113, 10712-10717.	3.1	82
77	Spontaneous construction of photoactive hollow TiO <sub>2</sub> microspheres and chains. Nanotechnology, 2009, 20, 325606.	2.6	73
78	Effect of PSS on morphology and optical properties of ZnO. Journal of Colloid and Interface Science, 2008, 326, 433-438.	9.4	95
79	Electrochemical properties of TiO2 hollow microspheres from a template-free and green wet-chemical route. Journal of Power Sources, 2008, 180, 869-874.	7.8	45
80	Cooperative self-construction and enhanced optical absorption of nanoplates-assembled hierarchical Bi2WO6 flowers. Journal of Solid State Chemistry, 2008, 181, 1048-1055.	2.9	131
81	Effects of calcination temperatures on photocatalytic activity of SnO2/TiO2 composite films prepared by an EPD method. Journal of Hazardous Materials, 2008, 154, 1141-1148.	12.4	188
82	Enhanced Photocalytic Activity of Hollow Anatase Microspheres by Sn <sup>4+</sup> Incorporation. Journal of Physical Chemistry C, 2008, 112, 2050-2057.	3.1	96
83	Novel preparation and photocatalytic activity of one-dimensional TiO2hollow structures. Nanotechnology, 2007, 18, 065604.	2.6	56
84	Effects of polyvinylpyrrolidone and cetyltrimethylammonium bromide on morphology of lead tungstate particles. Journal of Alloys and Compounds, 2007, 433, 73-78.	5.5	13
85	Microstructures and photoactivity of mesoporous anatase hollow microspheres fabricated by fluoride-mediated self-transformation. Journal of Catalysis, 2007, 249, 59-66.	6.2	359
86	Template-free Hydrothermal Synthesis of CuO/Cu <sub>2</sub> O Composite Hollow Microspheres. Chemistry of Materials, 2007, 19, 4327-4334.	6.7	450
87	Poly(methacrylic acid)-mediated morphosynthesis of PbWO4 micro-crystals. Applied Physics A: Materials Science and Processing, 2007, 87, 113-120.	2.3	33
88	A sonochemical route to visible-light-driven high-activity BiVO4 photocatalyst. Journal of Molecular Catalysis A, 2006, 252, 120-124.	4.8	340
89	Sonochemical synthesis of nanocrystallite Bi2O3 as a visible-light-driven photocatalyst. Applied Catalysis A: General, 2006, 308, 105-110.	4.3	356
90	Silver vanadium oxides nanobelts and their chemical reduction to silver nanobelts. Journal of Crystal Growth, 2006, 293, 404-408.	1.5	22

#	Article	IF	CITATIONS
91	Polymer-directed large-scale synthesis of single-crystal vanadium oxide nanobelts. Materials Chemistry and Physics, 2006, 95, 206-210.	4.0	15
92	Controlled Synthesis of Novel Flower-shaped BaCrO4Crystals. Chemistry Letters, 2005, 34, 564-565.	1.3	10
93	Effects of PSMA additive on morphology of barite particles. Journal of Crystal Growth, 2005, 275, 572-579.	1.5	34
94	Facile fabrication of monodispersed mesoporous celestine particles with peanut-shaped morphology. Journal of Crystal Growth, 2005, 279, 461-465.	1.5	19
95	Fabrication and characterization of Ag–TiO2 multiphase nanocomposite thin films with enhanced photocatalytic activity. Applied Catalysis B: Environmental, 2005, 60, 211-221.	20.2	660